Optical Engineering

SPIEDigitalLibrary.org/oe

Conformal phased array aero-optical modeling and compensation

Matthew R. Whiteley
Stanislav Gordeyev

SPIE

Conformal phased array aero-optical modeling and compensation

Matthew R. Whiteley
MZA Associates Corporation
1360 Technology Ct., Suite 200
Dayton, Ohio 45430
E-mail: matthew.whiteley@mza.com

Stanislav Gordeyev
University of Notre Dame
Institute for Flow Physics and Control
Indiana, 46556

Abstract. The effect of subsonic turbulent boundary layer aero-optical disturbances on a conformal phased array for laser beam projection operating on a high-speed aircraft is considered. We employ a basic model for subsonic boundary layer disturbances developed by Cress et al. which is governed by the displacement thickness δ^* to bound the magnitude of the problem, to determine the basic phenomenology affecting phased array performance, and to quantify requirements for compensation of these disturbances in the array subapertures. We used $\delta^* = 15$ mm as a baseline value in quantifying phased array effects on a 7-aperture hexagonal array with 10 cm subapertures. Boundary layer piston and tilt disturbances dominate array effects, but higher-order disturbances are similar in magnitude to the differential piston over the array and 2× greater in magnitude than an upper bound on free-stream turbulence. Adaptive optics compensation of turbulent boundary layer disturbances in such a phased array requires error rejection bandwidths >1 kHz for high-fidelity array performance. [DOI: 10.1117/1.OE.52.7.071409]

Subject terms: aero-optics; phased array; boundary layer; wavefront error; adaptive optics.

Paper 121577SS received Oct. 29, 2012; revised manuscript received Jan. 25, 2013; accepted for publication Jan. 25, 2013; published online Feb. 28, 2013.

1 Introduction

This study addresses the effect of aero-optical disturbances for conformal aperture systems on high-speed aircraft. These optical systems are designed to blend with the outer mould line of the aircraft, and therefore would experience less degradation due to aero-optical disturbances compared to a conventional hemisphere-on-cylinder turret. The most likely candidates for such a conformal optical system would be a phased array architecture, where the effective projection or imaging aperture for the optical system is comprised of a collection of array elements or subapertures. In order to gain the full benefit of the distribution of apertures over the airframe, the phasing of these apertures must be maintained within a fraction of the operating wavelength.

While a conformal aperture system will not experience the extreme degradation typical of a laser turret configuration,[1] the optical system will however be subject to turbulent boundary layer disturbances[2] which develop over the skin of any aircraft system. Turbulent boundary layers arise as the air flow will have a velocity profile ranging from 0 near the aircraft surface to the free-stream velocity u_∞ a distance away from the surface beyond the limit of the boundary layer. The boundary layer thickness is typically quantified as the point at which the surface-layer velocity is $0.99u_\infty$. However, a more useful metric for quantifying turbulent boundary layer effects is the *displacement thickness* δ^*, which is computed from the density profile $\rho(y)$ and velocity profile $u(y)$ for a given free-stream air density ρ_∞ as

$$\delta^* = \int_0^\infty \left[1 - \frac{\rho(y)u(y)}{\rho_\infty u_\infty}\right] \mathrm{d}y. \tag{1}$$

At low speed the velocity profile will be laminar, but as speed increases the flow within the boundary layer will become turbulent. The Reynolds number Re is typically used to quantify the degree to which a turbulent condition exists, and is calculated as

$$\mathrm{Re} = \rho_\infty u_\infty x/\mu_\infty, \tag{2}$$

where μ_∞ is the free-stream viscosity of air and x is a downstream location on the aircraft. Given the Reynolds number, the displacement thickness for a downstream location relative to the tip of the aircraft is computed as

$$\delta^* = 0.0463\, x\mathrm{Re}^{-0.2}. \tag{3}$$

The displacement thickness computed according to Eq. (3) with $x = 10$ m is shown in Fig. 1. To relate δ^* to flight conditions, we have plotted contours of δ^* with platform altitude, h versus Mach number, M. For each altitude considered, we compute the free-stream pressure $P_\infty(h)$, density $\rho_\infty(h)$, and temperature $T(h)$ according to the *U.S. Standard 1976* model.[3] Then, for a given altitude and Mach number, the free-stream velocity $u_\infty(h)$ is computed as

$$u_\infty(h) = M\sqrt{1.4P_\infty(h)/\rho_\infty(h_p)}. \tag{4}$$

The free-stream viscosity for each altitude is computed as[4]

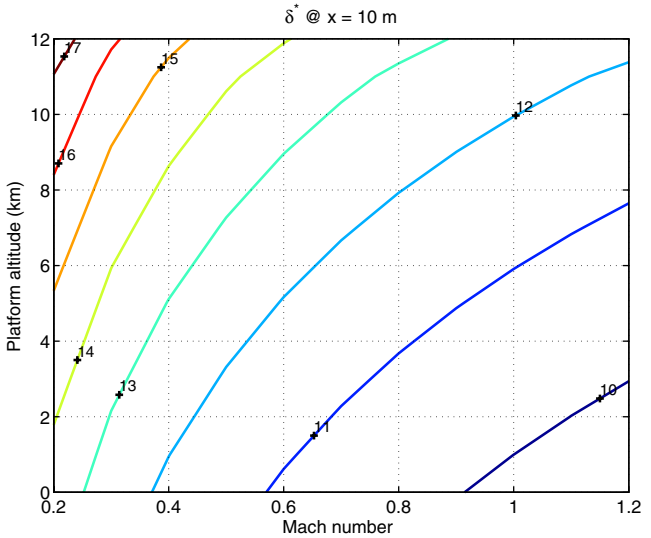

Fig. 1 Displacement thickness for location $x = 10$ m over a range of Mach numbers and platform altitudes.

$$\mu_\infty(h) = [1.458\ \mu\text{Pa s K}^{-1/2}]\frac{T(h)^{3/2}}{T(h) + 110.3\ \text{K}}. \quad (5)$$

Given these quantities, Re is computed according to Eq. (2) and used in Eq. (3) for δ^*. As the contours of Fig. 1 illustrate, for platform altitudes in the range of 5 to 10 km and Mach numbers in the range of 0.5 to 1.0, the interval of δ^* values is relatively small, ranging from 10 to 13 mm. Thus, in this regime variation in the displacement thickness is will be related more to airframe geometry than atmospheric properties.

The displacement thickness δ^* has been shown to be a fundamental scaling parameter for the optical properties of turbulent boundary layers.[5] These observations have led researchers, primarily Gordeyev et al. at the University of Notre Dame to develop particular modeling methods for turbulent boundary layers which are reviewed in Sec. 2. Using Gordeyev's basic modeling method, we have applied such boundary layer aero-optical disturbances to the problem of conformal aperture arrays in Sec. 3, quantifying the modal statics over such an array for a range of relevant δ^*. We then consider the compensation of turbulent boundary layer aero-optical disturbances for a conformal phased array system, quantifying the temporal properties of these disturbances and the bandwidth requirements for adaptive optics (AO) correction of such disturbances in an example array. We draw conclusions in Sec. 5.

2 Turbulent Boundary Layer Aero-Optical Wavefront Modeling

To address the influence of turbulent boundary layer disturbances on conformal apertures, we have patterned our work after the empirical scaling relations developed by Cress and Gordeyev at the University of Notre Dame.[2,6] In their approach, the random wavefront error associated with subsonic boundary layer aero-optics with adiabatic wall conditions has been observed to scale as

$$\sigma_{\text{BL}} = 1.65 \times 10^{-5}\delta^*(\rho_\infty/\rho_{\text{SL}})M^2, \quad (6)$$

where ρ_{SL} is air density at sea level, M is the free-stream Mach number, and δ^* is the displacement thickness as defined in Eq. (1). Equation (6) is valid for propagation perpendicular to the surface, i.e., perpendicular to the turbulent boundary layer. When propagating off-normal, it has been shown in other studies[7] that Eq. (6) can be extended considering β, the angle between the surface and the propagation direction, as in Eq. (7).

$$\sigma_{\text{BL}} = 1.65 \times 10^{-5}\delta^*(\rho_\infty/\rho_{\text{SL}})M^2/\sin(\beta). \quad (7)$$

This modification is simply a geometric scaling of the displacement thickness as the angle of propagation off perpendicular is increased. Although the precise scaling with propagation angle is complicated by the anisotropic nature of the boundary layer vortices, empirical studies have shown these relationship to hold in an approximate sense over a range of test angles.[2] The scaling model of Eq. (7) has been recently reexamined in the light of new data available for supersonic boundary layers, and a modification has been proposed for both subsonic and supersonic boundary layers.[5] The work with supersonic boundary layers is preliminary at this time and based on a single supersonic measurement. Given the range of flight conditions being considered here, we have elected to use the previously reported observations for subsonic boundary layers to study conformal array aero-optics.

To put Eq. (7) into context for the conformal phased array operating on a high-speed aircraft, consider the plots shown in Fig. 2. Figure 2(a) shows contours of rms wavefront error (WFE) for the same range of Mach number and altitudes which accompany the δ^* values in Fig. 1. Equivalently, if we consider a platform at 5 km altitude, Fig. 2(b) shows the WFE for a range of displacement thicknesses and different Mach numbers. The calculations of turbulent boundary layer WFE were made assuming propagation at $\beta = 45$ deg through the layer. As is shown in Fig. 2, the random WFE can easily reach a non-negligible level for an optical system operating near $\lambda = 1\ \mu$m wavelength. For instance, with $\delta^* = 15$ mm on a Mach 1.0 aircraft, $\sigma_{\text{WFE}} \simeq 0.2\ \mu$m, a level detrimental to optical performance if not compensated through AO methods. The updated boundary layer modeling which extends into supersonic regimes[5] would yield a lower WFE value of $\sigma_{\text{WFE}} = 0.15\ \mu$m which is still a significant optical degradation.

To place these considerations in the context of a distributed aperture system, we must not only consider the magnitude of the turbulent boundary layer optical disturbances, but also the spatial distribution. Cress and Gordeyev have developed a method of simulating phase screens for turbulent boundary layers which uses a standard fast Fourier transform (FFT)-based filtering technique assumes the spatial power spectrum of disturbances follows standard scaling relations with δ^* as have been observed in detailed wavefront studies.[6,8] Notably, the disturbances in the stream-wise direction have a longer correlation length than in the cross-stream direction. In these studies it was found that the stream-wise correlation length was $5.2\delta^*$ whereas the span-wise correlation length was $0.75\delta^*$. The key observation of importance in the modeling is that the displacement thickness also sets the scale size of the optical disturbances in addition to establishing the strength of disturbances according to Eq. (7). Once random phase screen realizations which the

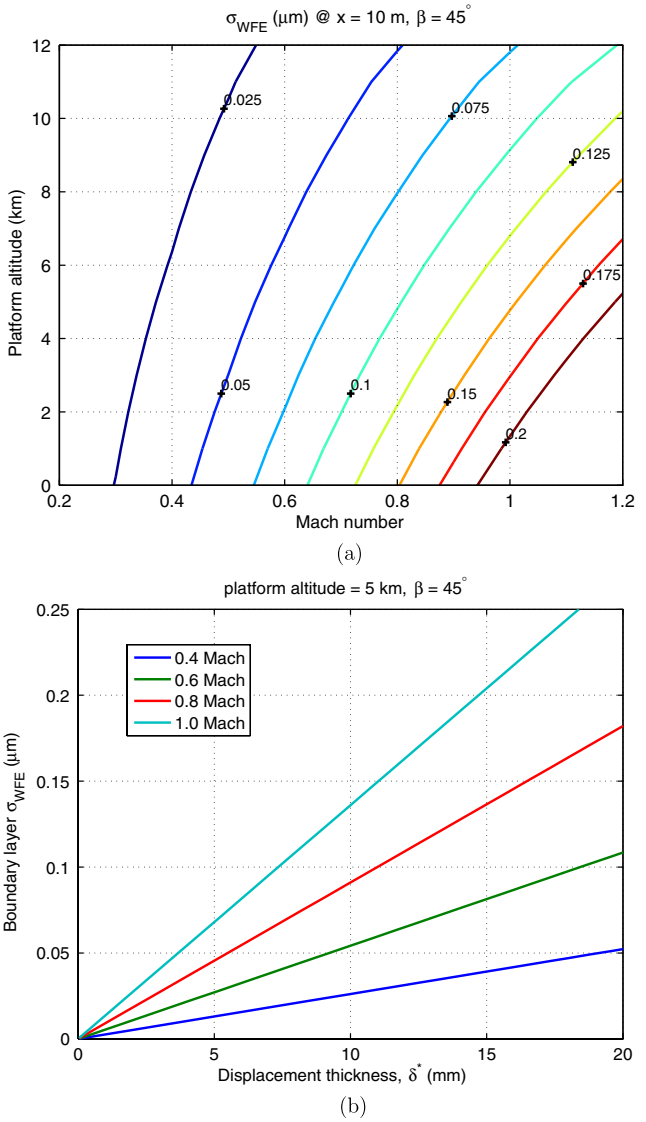

Fig. 2 Turbulent boundary layer wavefront error for a platform at 5 km altitude as a function of boundary layer displacement thickness δ^* for various Mach numbers.

proper power and spatial scale (set by δ^*) are generated, these disturbances can be used as phase screens in a wave-optics simulation. To simulate temporal dynamics of the boundary layer disturbance, the simulated phase screen can be translated at a convention rate which is approximately $0.8u_\infty$, as has been observed in the fundamental measurements supporting the modeling approach.[7]

3 Aero-Optical Mode Statistics in a Conformal Aperture Array

Using the turbulent boundary layer model presented in Sec. 2, we will now quantify the effect of these aero-optical disturbances on a 7-aperture conformal array pattern, as shown in Fig. 3. Figure 3 shows the aperture array configuration with 10 cm subapertures separated by 12 cm center-to-center in a hexagonal pattern often-referred to as "hex-7." In this configuration, the array can be inscribed within a circle of 35 cm diameter (dashed line). The images in Fig. 4 show

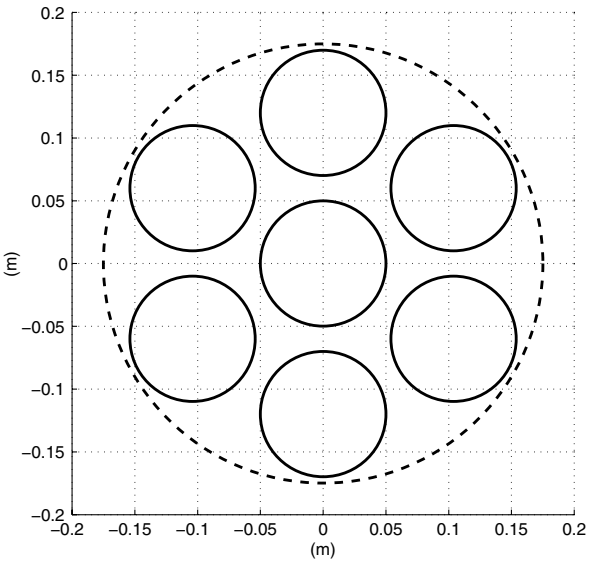

Fig. 3 Hex-7 aperture array used for boundary layer aero-optical effects evaluation.

phase disturbances in the apertures for $\delta^* = 1, 2, 5, 10$ mm. It is interesting to note both the magnitude and scale size of boundary layer disturbances within each subaperture. For small values of δ^* the disturbance scale is small compared to the aperture, but also low in magnitude. As δ^* increases, the differential "piston" phase between apertures increases notably. However, there is more correlation of phase effects between the apertures. This observation indicates that although the disturbances on a conformal array will be more severe further back on the aircraft, these disturbances may be more correctable by an appropriate laser phasing approach.

For the purpose of quantifying the modal statistics of boundary layer disturbances, we designated the center subaperture to be the "master" aperture in the array. In an operable phased array, the entire array is phased up to this master subaperture. Two of the key metrics of interest for such an array is the differential piston and tilt terms for the array apertures relative to the master. Figure 5 shows the standard deviation of the piston and tilt of the array elements relative to the master for the hex-7 array pattern as a function of δ^*. To quantify these statistics, we generated 500 realizations of boundary layer aero-optical disturbances for each of the δ^* values. The piston and tilt from each aperture where projected from the wavefront when the array was overlaid onto the phase screen. The piston and jitter from the master aperture was differenced with the piston and jitter from each array element, respectively. The quantities shown in Fig. 5 are the standard deviation of this differential piston or jitter term.

From Fig. 5(a) we see that the differential piston term in the array exceeds 100 nm ($\lambda/10$ for a nominal $\lambda = 1$ μm) for $\delta^* > 10$ mm. The differential piston grows linearly with δ^* as this parameter governs the overall magnitude of the aero-optical boundary layer disturbance. Figure 5(b) shows the differential jitter components for the same set of boundary layer aero-optical wavefronts. We see that the jitter components also scale linearly with δ^*, similarly to the piston term. However, we also see that jitter in the "Y"-axis is larger than

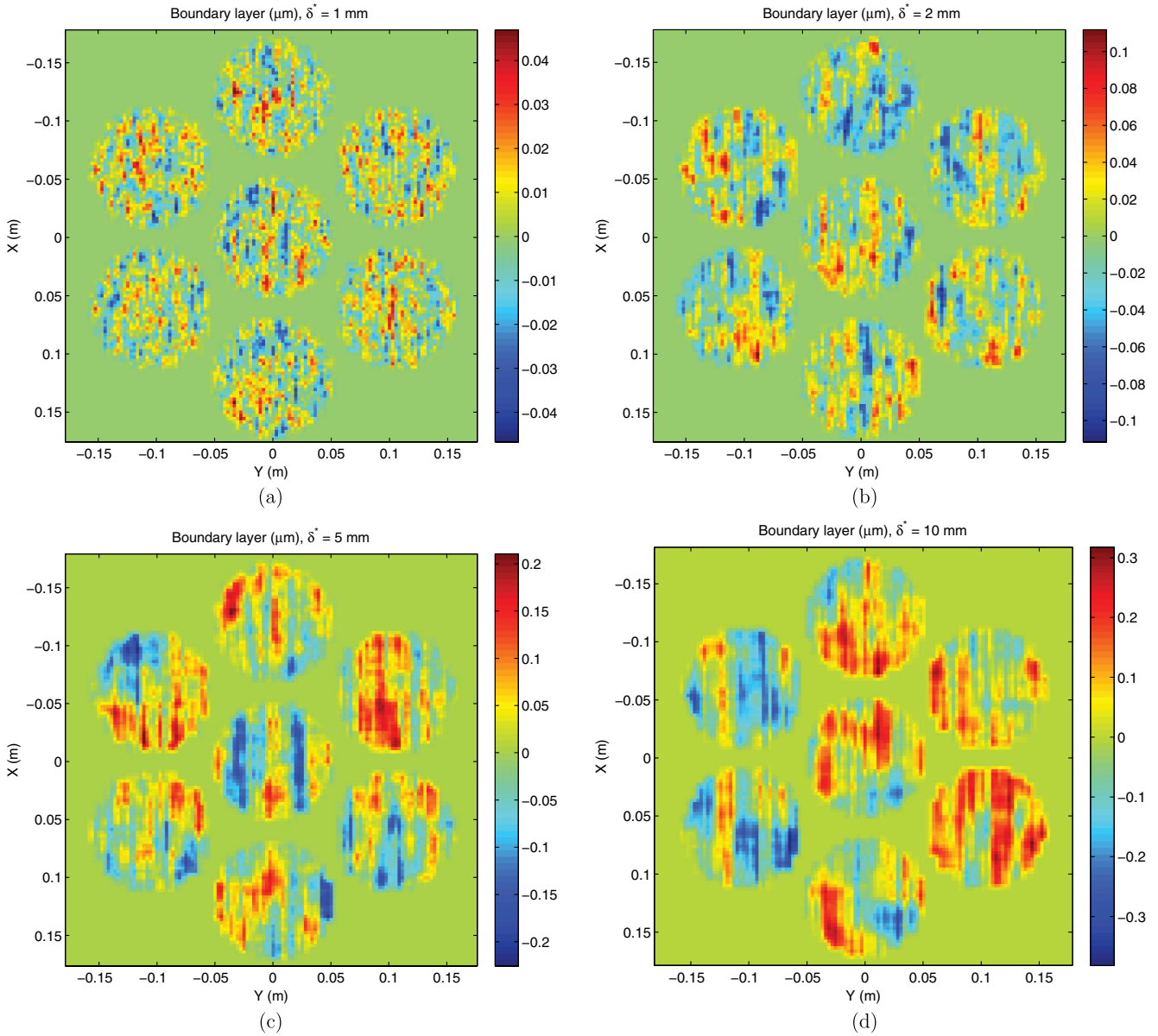

Fig. 4 Boundary layer phase screen realizations with variable displacement thickness δ^* for an aperture array with 10 cm subapertures in a hex-7 pattern with 12 cm aperture spacing. (a) $\delta^* = 1$ mm, (b) $\delta^* = 2$ mm, (c) $\delta^* = 5$ mm and (d) $\delta^* = 10$ mm. Phase screen realizations have been generated for a platform at 5 km altitude with 1.0 Mach airspeed under standard atmospheric conditions.

jitter in the "X"-axis by approximately 50%. In our coordinate convention, the Y-axis is aligned in the flow direction whereas the X-axis is aligned with the cross-flow direction. As noted previously, boundary layer aero-optical disturbances have a characteristic scale size which is asymmetric and longer in the flow direction than in the cross-flow direction. This results in the asymmetry of jitter effects quantified in Fig. 5(b).

4 Compensation of Aero-Optical Disturbances on Conformal Phased Arrays

The degradation of conformal array optical performance in the presence of boundary layer aero-optical disturbances is of primary interest for the current study. We also want to quantify the performance of such an array when tilt and piston are corrected within each aperture since these phase modes are commonly corrected by the transmit-laser-phasing beam control. To quantify these effects, we generated random disturbances like those shown in Fig. 4(b) for the hex-7 aperture array and for varying values of δ^*. For each realization, the phase disturbance was applied to the array and the array was brought to a focus to model the point spread function (PSF) of the array. This process was repeated for an ensemble of boundary layer aero-optical phase screens. For each phase screen realization, we also removed the tilt components only, the piston-components only, and the combination of tilt and piston components. This allowed us to simulate the array PSF with these components removed. The PSFs where averaged over an ensemble of 32 phase screen realizations to simulate the average PSF, which would be proportional to the average transmit irradiance achievable with such an array given the boundary layer properties.

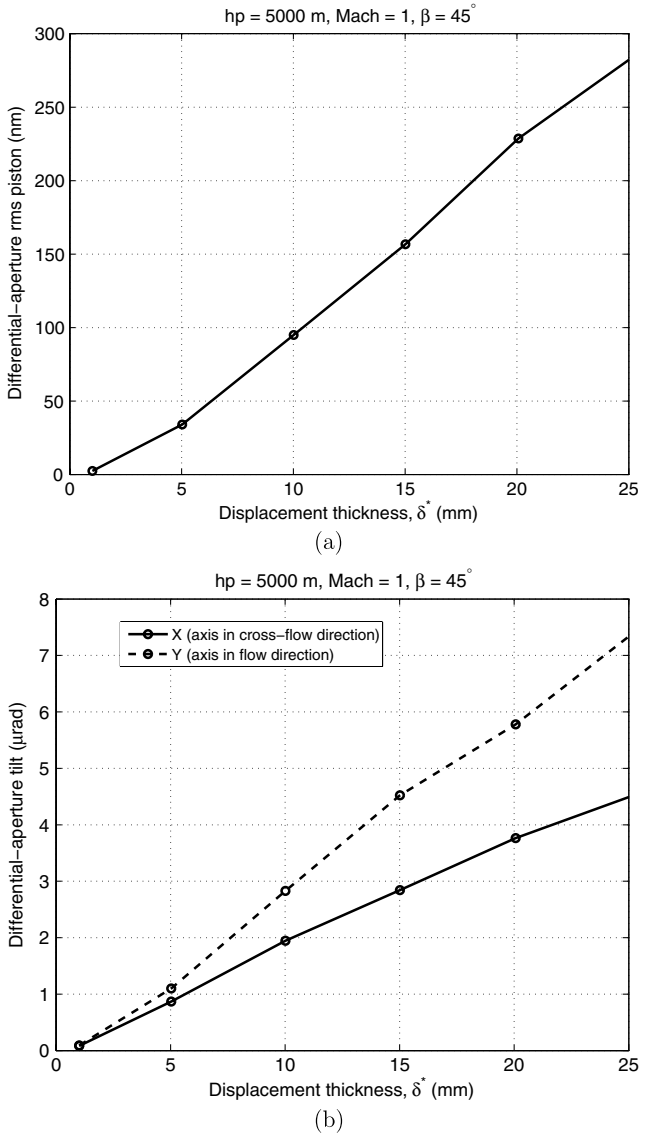

Fig. 5 Magnitude of aperture modal phase disturbances for hex-7 array evaluated at 5 km platform altitude with 1.0 Mach airspeed. (a) Differential piston for subapertures relative to master. (b) Differential jitter for subapertures relative to master.

Figure 6 shows the PSFs for $\delta^* = 10$ to 25 mm for the hex-7 array. The sequence of images shows (from left to right) open-loop (no compensation), tilt-only correction, piston-only correction, tilt + piston correction, and vacuum propagation. The image sequences have been normalized to the PSF with vacuum propagation so the color scale is proportional to the Strehl intensity in all the images. We note that with no piston or tilt correction, the array Strehl ratio is less than 0.5 for $\delta^* > 10$ mm and becomes elongated in the cross-flow direction due to the asymmetry of the boundary layer phase structures. We note that neither tilt-only nor piston-only compensation alone provides for robust central core irradiance formation. Only when both tilt and piston are compensated over the array do we see a well-formed core at all values of δ^* considered.

Figure 7(a) shows numerically the Strehl values of the open-loop, tilt-only correction, piston-only correction, and tilt + piston-correction for the array. These plots illustrate that piston correction is more effective than tilt correction at improving beam projection from the array. However, neither tilt nor piston alone provides an effective compensation for the array disturbances. When both tilt and piston correction are applied to the array, we see a substantial increase in the array Strehl ratio. However, we note that for $\delta^* = 25$, the compensated Strehl ratio is less than 0.4 for the array, indicating a moderately strong higher-order disturbance in the array due to boundary layer aero-optics.

Figure 7(b) shows the same data as in Fig. 7(a) but cast in terms of "apparent" wavefront error using an inverse Marechal approximation method

$$\sigma'_{\mathrm{WFE}} = (\lambda/2\pi)\sqrt{-\log(S)}, \tag{8}$$

where λ is the transmitted wavelength ($\lambda = 1$ μm in this case) and S is the Strehl ratio observed in the simulations. For comparison to the applicable theory, we have plotted Eq. (7) as the dashed line in Fig. 7(b). First, we see that the apparent effect of boundary layer disturbances for open-loop propagation from an array departs from the Marechal approximation at larger values of δ^*. This is to be expected since the wavefront error grows beyond the applicable limit for validity of the Marechal approximation. However, we note that when tilt and piston are removed from the wavefront, the residual wavefront error is nonlinear with δ^*. We also note that for $\delta^* = 25$ mm, the tilt and piston-removed wavefront error is greater than 50% of the uncorrected disturbance. Thus, the majority of wavefront disturbances for the 10 cm apertures assumed in our simulations does not present itself as tilt or piston within the array apertures. These higher-order disturbances would require more degrees of freedom in the laser phasing beam control system in order to be substantially compensated.

4.1 *Temporal Properties of Boundary Layer Disturbances in a Conformal Phased Array*

We now address the temporal properties of the modal wavefront statistics in the hex-7 aperture array, and address the required error rejection bandwidth for compensating boundary layer disturbances. To carry out this analysis, the same boundary layer phase screen generator was used as employed in the previous analysis, but this time to generate a correlated time history of boundary layer phase screens instead of random samples. In the modeling, the basic assumption used to simulate temporal evolution is that the convective velocity of the boundary layer disturbances is ~0.8× the free-stream velocity, i.e., $u_c \simeq 0.8u_\infty$, as has been shown empirically from high-speed Malley probe measurements.[2,9] For the current analysis, we assume an aircraft boundary layer on a platform at 5 km altitude with 1.0 Mach airspeed. The disturbances are computed for light passing through the boundary layer at angle $\beta = 45$ deg to the normal of the outer mould line of the aircraft. These disturbances scale as $1/\sin\beta$ due to the propagation path length through the boundary layer. The conditions noted here are applied consistently for the results in the remainder of this section.

Given the flight conditions noted above, and assuming a displacement thickness of $\delta^* = 15$ mm, a time history of boundary layer wavefront was simulated at a sample rate of 20 kHz. For each wavefront sample in the time history,

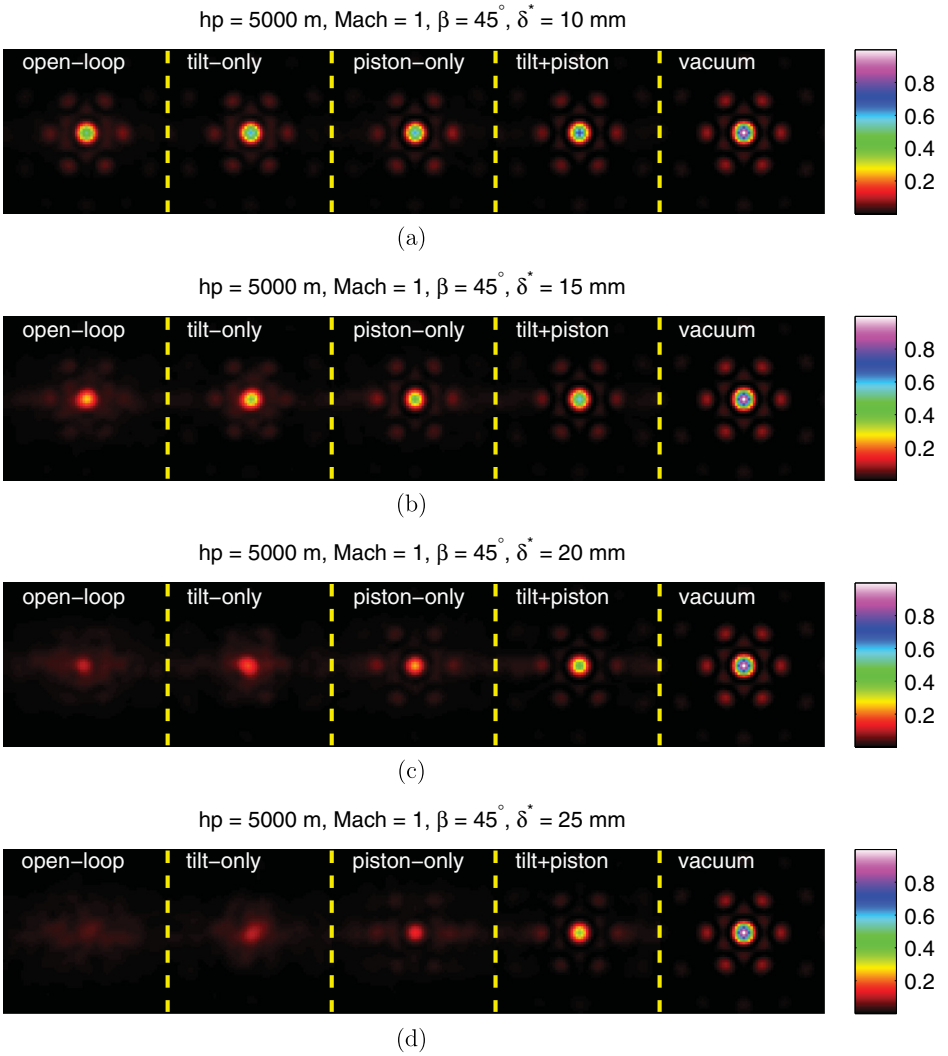

Fig. 6 Point spread functions associated with the 7-aperture conformal array affected by boundary layer aero-optical disturbances. (a) $\delta^* = 10$ mm, (b) $\delta^* = 15$ mm, (c) $\delta^* = 20$ mm, and (d) $\delta^* = 25$ mm. All evaluations are for a platform at 5 km altitude traveling at Mach 1.0 airspeed.

the piston and tilt components were computed, then removed from the wavefront, yielding a higher-order-only wavefront in the 10 cm subaperture. For comparison, we also retained the full-phase time history for the original wavefront disturbance. Figure 8(a) shows the temporal power spectral density (PSD) and Fig. 8(b) shows the root of the forward-sum of the PSD (cumulative WFE) for the subaperture piston. These results show that most of the disturbance is below 1 kHz, and a substantial portion of the piston disturbance is below 500 Hz.

Figure 9(a) shows the temporal PSD and Fig. 9(b) shows the root of the forward-sum of the PSD for the subaperture tilt. The jitter for each subaperture is asymmetric with the larger component being about an axis which is in the flow direction; the axis we have identified as "Y" in our analysis. This is due primarily to the asymmetric correlation lengths noted in boundary layer measurements where the correlation length is approximately $5.2\delta^*$ in the streamwise direction and approximately $0.75\delta^*$ in the cross-stream direction, as discussed in Sec. 2. Note that in comparing the power spectrum of the jitter components that the larger axis of jitter has more power at lower frequencies as compared with the smaller axis of jitter. For reference, the mid-point in cumulative jitter for the X-jitter is approximately 600 Hz, whereas for the Y-jitter the mid-point in cumulative jitter is less than 100 Hz.

Figure 10(a) shows the temporal PSD of the piston and tilt-removed phase. Figure 10(b) shows the cumulative WFE associated with this power spectrum. For comparison, we have also plotted the PSD and cumulative WFE for the full phase (including piston and tilt) over the subaperture. We note that removal of piston and tilt from the subaperture phase suppresses wavefront disturbances at frequencies $f < 0.5u_c/d \simeq 1700$ Hz, where d is the subaperture diameter. However, the residual WFE after removing piston and tilt from the subaperture is a substantial fraction of the full disturbance, accounting for more then 60% of the boundary layer WFE. Thus, while compensation of the subaperture piston in a phased array is an important beam control function, the influence of higher-order disturbances on array performance is not negligible. To place this disturbance level into context, we consider that for a well-chosen phased array subaperture, then $d/r_0 < 1$, where r_0 is the atmospheric coherence diameter for free-stream atmospheric

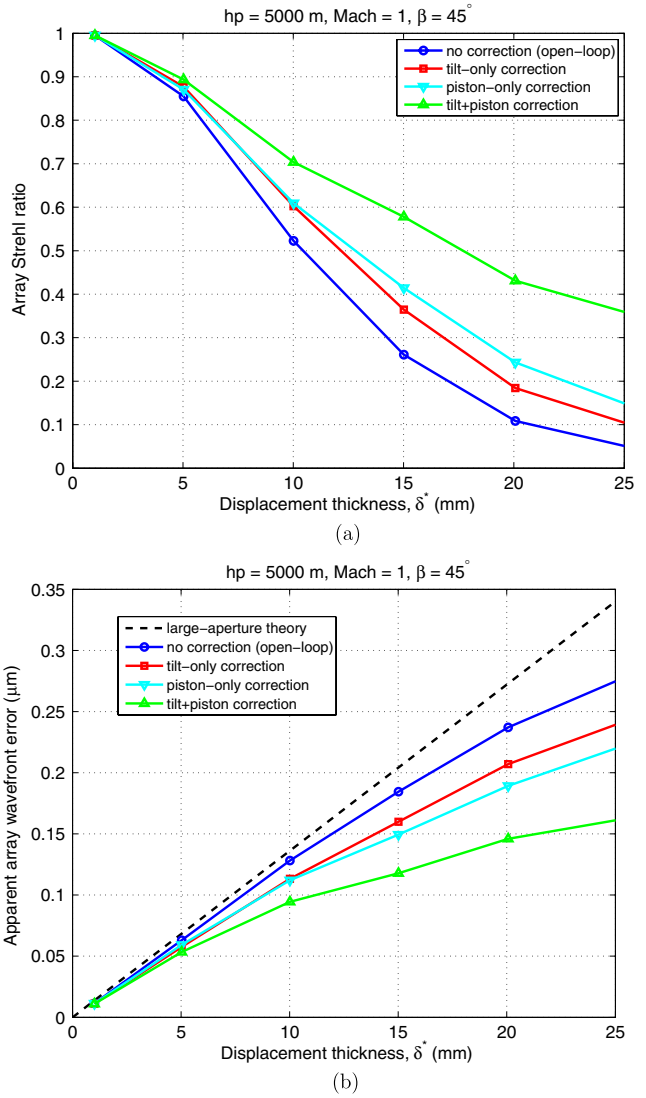

Fig. 7 Conformal aperture performance metrics with boundary layer aero-optical disturbances derived from array point-spread functions. (a) Strehl ratio. (b) Apparent wavefront error. Plots show open-loop compared to tilt-only correction, piston-only correction, and tilt + piston correction.

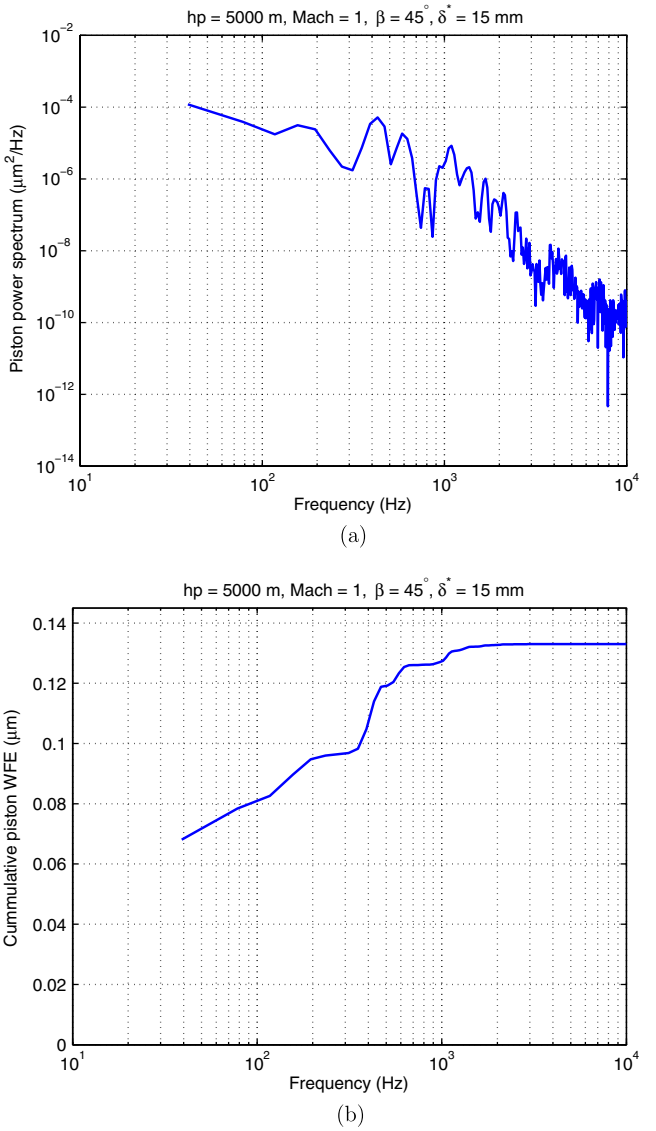

Fig. 8 Temporal statistics of 10 cm subaperture piston for 5 km platform altitude with 1.0 Mach airspeed with $\delta^* = 15$ mm. (a) Temporal power spectrum. (b) Forward sum of temporal power spectrum presented as cumulative WFE.

turbulence.[10] In this condition, an upper bound on the piston and tilt-removed wavefront variance is 0.134 rad^2,[11] which for $\lambda = 1$ μm wavelength is equivalent to $\sqrt{0.134}\times\lambda/(2\pi) = 0.06$ μm. Thus, the subaperture piston and tilt-removed WFE of 0.12 μm for boundary layer aero-optics in the flight condition examined is twice as large as free-stream atmospheric disturbances.

4.2 *Temporal Bandwidth Requirements for Compensating Boundary Layer Aero-Optical Disturbances*

To address the implications of the temporal statistics for boundary layer aero-optical disturbances as reported in Sec. 4.2, we follow the standard error rejection modeling approach we have applied previously to other aero-optical data.[12–14] The analysis assumes the use of a classical discrete integrator control law where the control commands c at time t_{k+1} are given by

$$c(t_{k+1}) = c(t_k) + \beta\epsilon(t_k), \tag{9}$$

where β is the loop gain applied to the reconstructed wavefront error $\epsilon(t_k)$ at each time step t_k. If the control system has no latency and the response time of the mirror is instantaneous, then the error rejection function for the controller is modeled as

$$\mathrm{ERJ}(f; f_{3\mathrm{dB}}) = \left[1 + \left(\frac{f}{f_{3\mathrm{dB}}}\right)^{-2}\right]^{-1}, \tag{10}$$

where the error rejection bandwidth $f_{3\mathrm{dB}}$ is commonly[15,16] defined as

$$f_{3\mathrm{dB}} \equiv \frac{\beta f_s}{2\pi}, \tag{11}$$

and f_s designates the sampling frequency of the discrete-time system. Given the error rejection function for the

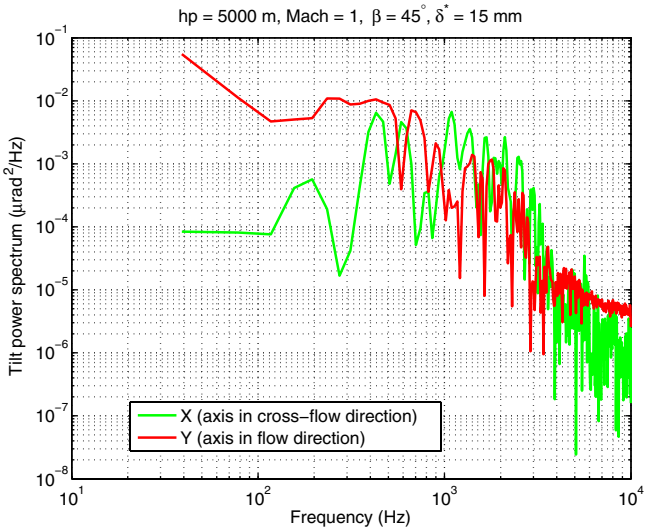

(a)

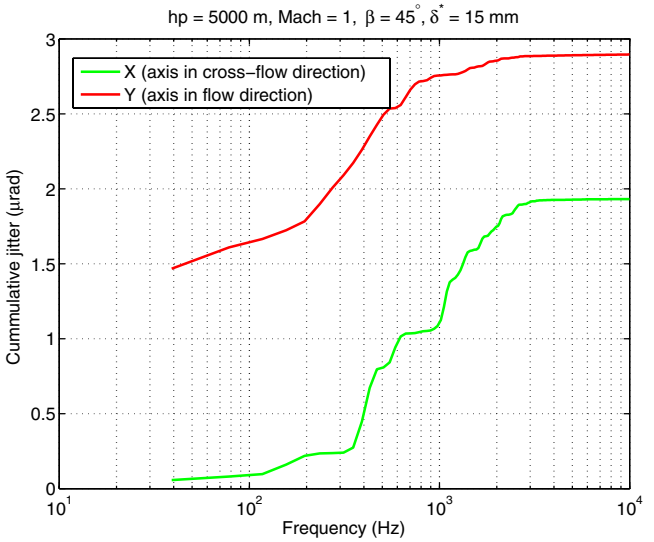

(b)

Fig. 9 Temporal statistics of 10 cm subaperture tilt for 5 km platform altitude with 1.0 Mach airspeed with $\delta^* = 15$ mm. (a) Temporal power spectrum. (b) Forward sum of temporal power spectrum presented as cumulative jitter.

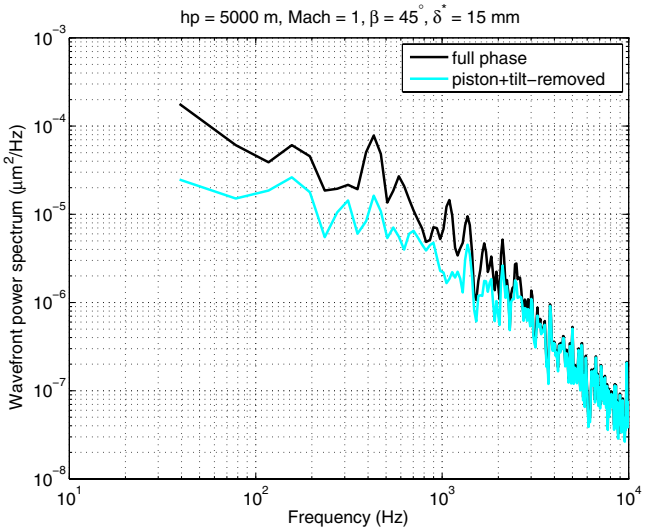

(a)

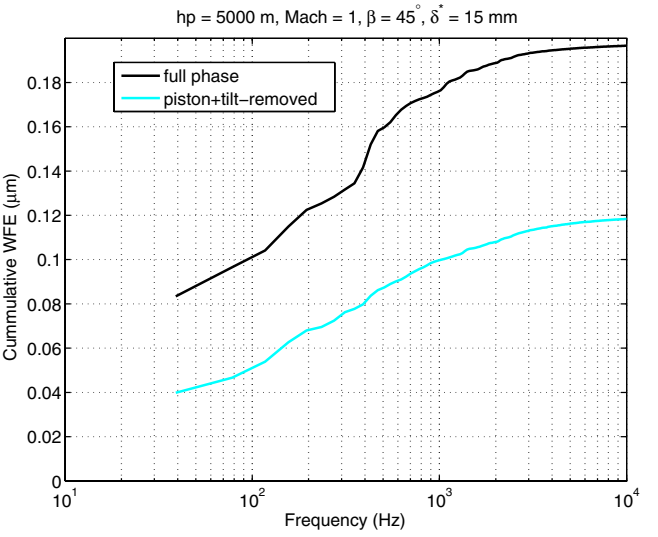

(b)

Fig. 10 Temporal statistics of 10 cm subaperture higher-order phase for 5 km platform altitude with 1.0 Mach airspeed with $\delta^* = 15$ mm. (a) Temporal power spectrum. (b) Forward sum of temporal power spectrum, presented as cumulative WFE. Higher-order statistics are plotted with the full-phase (including piston and tilt) for comparison.

classical AO controller in Eq. (10), the residual phase variance for a particular disturbance can be computed as

$$\varepsilon^2_{\text{res}} = \int_0^\infty \text{ERJ}(f; f_{3\text{dB}}, \Delta t)\Phi_d(f)\text{d}f, \tag{12}$$

where $\Phi_d(f)$ is the temporal PSD of the disturbance to be compensated, in this case the modal or higher-order disturbances from the conformal boundary layer aero-optics.

Figure 11 shows the application of this compensation model to the aero-optical disturbances for two different conformal boundary layer cases. Again we assumed a 5 km platform altitude and 1.0 Mach airspeed. The compensation results are shown for $\delta^* = 5$ mm in Fig. 11(a) and $\delta^* = 15$ mm in Fig. 11(b). The plots illustrate the reduction in phase variance as a function of $f_{3\text{dB}}$ for the control system, relative to the uncompensated ($f_{3\text{dB}} = 0$) condition. Curves are shown in the plots for piston-only, X-tilt, Y-tilt, and for the higher-order (piston and tilt removed) phase.

To indicate the error rejection bandwidth requirement for the disturbances, we have included a dashed black line where the residual variance is 0.25× the open-loop condition, i.e., where wavefront error or jitter is reduced by 1/2. Thus, the frequency at which each curve falls below 0.25 is taken to be the minimum bandwidth requirement for compensation of the disturbances. From Fig. 11(a) for $\delta^* = 5$ mm we see that piston compensation has the lowest bandwidth requirement, but requires an error rejection bandwidth of approximately 750 Hz. The bandwidth requirement for Y-tilt (axis aligned with flow direction) is slightly higher, but is less than 1 kHz. (Note that compensating the orthogonal jitter axis requires significantly higher bandwidth $f_{3\text{dB}} \simeq 3$ kHz.) Fortunately, this is the axis with lower jitter for the boundary

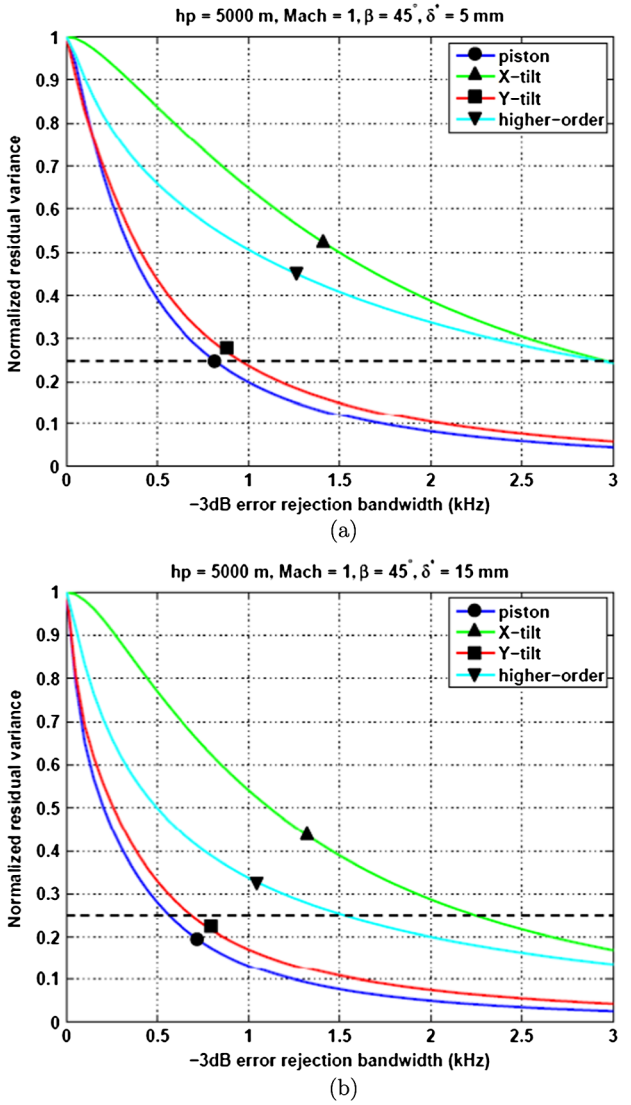

Fig. 11 Compensation of phase variance with control error rejection (−3 dB) bandwidth for a 10 cm subaperture on a 5 km platform altitude and 1.0 Mach airspeed. (a) $\delta^* = 5$ mm and (b) $\delta^* = 15$ mm. Plots show residual phase variance normalized to open-loop ($f_{-3\text{dB}} = 0$). Dashed line shows normalized residual variance of 0.25, i.e., where wavefront error or jitter is reduced by 1/2.

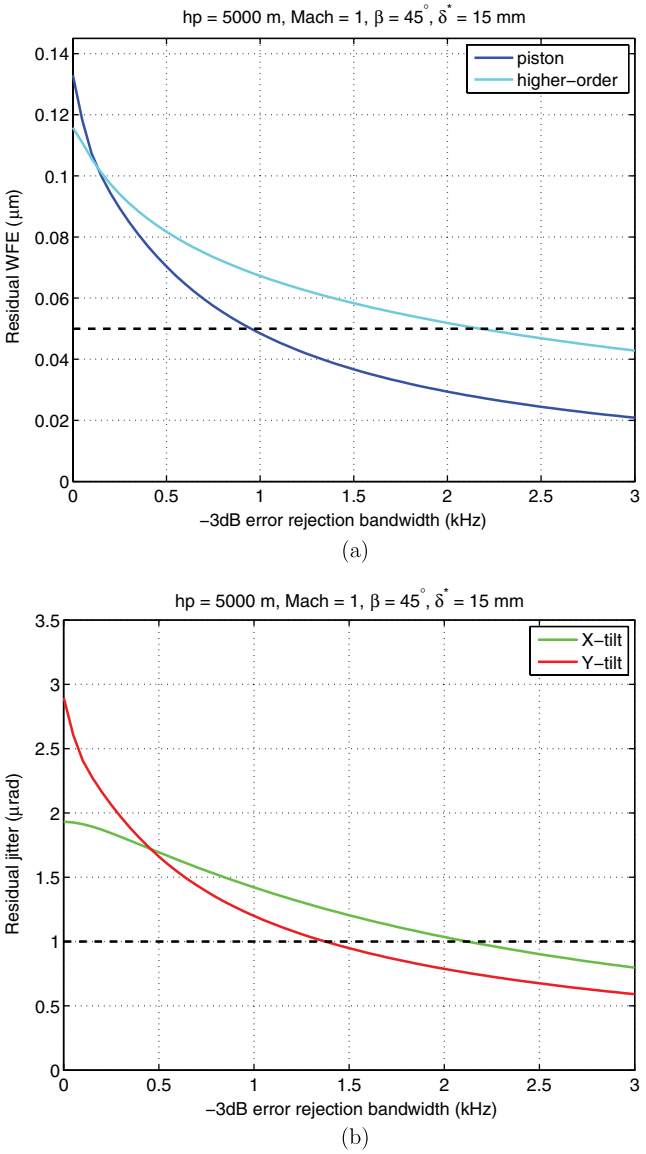

Fig. 12 Residual aero-optical disturbance modes with control error rejection (−3 dB) bandwidth for a 10 cm subaperture on a 5 km platform altitude and 1.0 Mach airspeed with $\delta^* = 15$ mm. (a) Piston and higher-order residual wavefront error. (b) Residual subaperture jitter.

layer disturbance. In order to compensate higher-order disturbances, the required bandwidth is approximately 3 kHz.

Figure 11(b) shows the relative residual error for compensation for $\delta^* = 15$ mm. In this case, we see that the bandwidth requirements to reach the same error relative to open-loop have dropped considerably compared to $\delta^* = 5$ mm. For instance, the equivalent bandwidth for higher-order compensation is $f_{3\text{dB}} \simeq 1.5$ kHz; less than half of the comparable value for $\delta^* = 5$ mm. It is interesting to note that the bandwidth requirements are lower for the larger values of δ^*, if the requirement is cast in terms of the residual being a fraction of the total. But since the magnitude of wavefront disturbances scales up linearly with δ^* (variance scales with δ^{*2}) the actual bandwidth required to reach an arbitrary set residual WFE will overall be higher as δ^* increases. To illustrate this point, consider the absolute value of the residual piston, tilt, and higher-order disturbances in Fig. 12 for the case of $\delta^* = 15$ mm. If an arbitrary residual error of 0.05 μm were set for piston and higher-order compensation, then the error rejection bandwidth to reach this residual disturbance level would need to be 1 kHz for piston and approximately 2 Hz for higher-order disturbances. Likewise, to reach an arbitrary residual jitter of 1 μrad for both tilt axes, the error rejection bandwidth would need to be 1.5 to 2 kHz. It is important to note here that achieving such error rejection bandwidths typically requires 10 to 20× oversampling in a feedback control system. Thus, feedback sensor sample rates of 20 to 40 kHz may be required to compensate these disturbances.

5 Conclusions

Conformal-aperture implementation of a laser beam director reduces many of the large-magnitude aero-optical effects for turrets. An optical setup consisting of an array of projection apertures which are phased to produce irradiance levels

similar to a full aperture system are an attractive option for laser systems on high-speed aircraft. Conformal arrays will still be subject to aero-optical disturbances resulting from the turbulent boundary layer on the aircraft surface. Theoretical models of boundary layer aero-optics have been validated through wind tunnel measurements which may be applied to analysis of conformal phased array performance and the AO compensation requirements for these disturbances.

Using available models, turbulent boundary layer wavefront disturbances were found to be $>\lambda/10$ (at $\lambda = 1$ μm) for aircraft speeds greater than Mach 0.8 over wide range of operating altitudes. Based on estimates of displacement thickness δ^* flight regimes of interest, $\delta^* = 15$ mm was employed in our phased array modeling for an aircraft at 5 km altitude at Mach 1.0. We used a 7-aperture hexagonal pattern of apertures with 10 cm diameter as a baseline in our modeling. These studies show turbulent boundary layer piston and tilt dominate and are nearly equal in effect on the phased array irradiance. Higher-order disturbances are nearly as strong as piston for this array configuration. These higher-order wavefront disturbances for boundary layer aero-optics were shown to be twice as large as the upper bound on free-stream disturbances in an ideally sized phased array subaperture. To achieve a residual error of 0.05 μm for piston and higher-order compensation, the error rejection bandwidth for a temporal feedback controller would need to be 1 kHz for piston and approximately 2 Hz for higher-order disturbances. For a residual jitter of 1 μrad, the error rejection bandwidth would need to be 1.5 to 2 kHz. Achieving such error rejection bandwidths in a feedback controller would require sensor sample rates of 20 to 40 kHz in a beam control system for the aircraft flight conditions analyzed here.

Acknowledgments

The authors acknowledge significant contributions of other collaborators at the University of Notre Dame (UND), notably Jacob Cress who provided code examples which were the basis for the phase screen modeling approach used in this project. This research was supported by the Air Force Research Laboratory (AFRL) Directed Energy Directorate under contract number FA9451-11-C-0191 and has been cleared for public release by the 377th Air Base Wing Office of Public Affairs, Kirtland AFB, New Mexico.

References

1. S. Gordeyev and E. Jumper, "Fluid dynamics and aero-optics of turrets," *Prog. Aerospace Sci.* **46**(8), 338–400 (2010).
2. J. Cress, S. Gordeyev, and E. Jumper, "Aero-optical measurements in a heated, subsonic, turbulent boundary layer," in *48th AIAA Aerospace Science Meeting and Ex-hibit*, Orlando, FL, pp. 4–7 (2010).
3. ADA-035728, *Handbook of Geophysics and the Space Environment, U.S. Standard Atmosphere, 1976*, National Oceanic and Atmospheric Administration, Washington, DC (1976).
4. Ames Research Staff, "Equations, tables and charts for compressible flows," Tech. Rep. NASA Report 1135 (1953), Reprinted by TechPress Publishing Co., North Olmstead, OH (1992).
5. S. Gordeyev, E. Jumper, and T. E. Hayden, "Aero-optical effects of supersonic boundary layers," *AIAA J.* **50**(3), 682–690 (2012).
6. J. A. Cress, "Optical aberrations caused by coherent structures in a subsonic, compressible, turbulent boundary layer," Ph.D. Thesis, University of Notre Dame, Notre Dame, IN (2010).
7. J. Cress et al., "Aero-optical measurements in a turbulent, subsonic boundary layer at different elevation angles," in *39th AIAA Plasmadynamics and Lasers Conf.*, Seattle, Washington, Vol. 4214, pp. 23–26 (2008).
8. D. J. Wittich, S. Gordeyev, and E. J. Jumper, "Revised scaling of optical distortions caused by compressible, subsonic turbulent boundary layers," in *38th AIAA Plasmady- namics and Lasers Conf.*, Miami, Florida, Vol. 4009, pp. 25–28 (2007).
9. S. Gordeyev, E. J. Jumper, and T. Hayden, "Aero-optics of supersonic boundary layers," in *AIAA 2011-1325* (2011).
10. D. L. Fried, "Optical resolution through a randomly inhomogeneous medium for very long and very short exposures," *J. Opt. Soc. Am.* **56**(10), 1372–1379 (1966).
11. M. C. Roggemann and B. Welsh, *Imaging Through Turbulence*, CRC Press, Boca Raton (1996).
12. M. R. Whiteley et al., "Adaptive controls for aero-optics and atmospheric compensation," Tech. Rep. AFRL-DE-PS-TR-2007-1044, Air Force Research Laboratory, Directed Energy Directorate, Kirtland AFB, New Mexico (2007), Contract Number FA9451-06-M-0128, MZA Associates Corporation.
13. M. R. Whiteley and J. S. Gibson, "Adaptive laser compensation for aero optics and atmospheric disturbances," in *38th AIAA Plasmadynamics and Lasers Conf.*, Vol. 4012 (2007).
14. M. R. Whiteley and R. J. Drye, "Adaptive controls for aero-optics and atmospheric compensation (phase II)," Tech. Rep. AFRL-RD-PS-TR-2010-1012, Air Force Research Laboratory, Directed Energy Directorate, Kirtland AFB, New Mexico (2010), Contract Number FA9451-07-C-0030, MZA Associates Corporation.
15. B. L. Ellerbroek, "First-order performance evaluation of adaptive-optics systems for atmospheric turbulence compensation in extended-field-of-view astronomical telescopes," *J. Opt. Soc. Am. A* **11**(2), 783–805 (1994).
16. G. A. Tyler, "Bandwidth considerations for tracking through turbulence," *J. Opt. Soc. Am. A* **11**(1), 358–367 (1994).

Matthew R. Whiteley received his MS (1995) and PhD (1998) in physics from the Air Force Institute of Technology. He received a BS in physics from Carnegie Mellon University in 1991. From 1998 to 2002, he was a deputy chief and advanced concepts team lead at the Airborne Laser Technology Branch of the U.S. Air Force Research Laboratory. From 2002 to 2005, he was a group leader and senior research scientist at Mission Research Corporation, and he is now a vice president and senior scientist at MZA Associates Corporation. His research interests include optical turbulence, aero-optical flow, adaptive optics, and wave-optics simulations.

Stanislav Gordeyev is a research associate professor in the Department of Aerospace and Mechanical Engineering, University of Notre Dame. He is an internationally recognized expert in investigating optical distortions caused by compressible turbulent flows around airborne systems. His expertise includes performing complex experimental investigations of optical aberrations, both in a time-averaged and instantaneous sense, in boundary layers, shear layers and wakes, as well as around complex geometries, like side-mounted turrets at subsonic and transonic speeds; experimental results and developed models are currently widely used to design laser airborne systems, as well to validate computational codes to predict optical distortions caused by turbulent flows. He is also actively involved in various studies of different mitigation techniques to improve the overall optical performance of airborne systems.